Electrochimica Acta 264 (2018) 341–349

Contents lists available at ScienceDirect

Electrochimica Acta

journal homepage: www.elsevier.com/locate/electacta

High-performance Li-Se battery cathode based on $CoSe_2$-porous carbon composites

Jun Yang [a], Hongcheng Gao [a], Dejun Ma [b], Jiasui Zou [a], Zhang Lin [c], Xiongwu Kang [a, *], Shaowei Chen [a, d, **]

[a] Guangzhou Key Laboratory for Surface Chemistry of Energy Materials, New Energy Research Institute, School of Environment and Energy, South China University of Technology, Guangzhou 510006, China
[b] School of Pharmacy, Guangdong Pharmaceutical University, Guangzhou 510006, China
[c] Guangdong Engineering and Technology Research Center for Environmental Nanomaterials, School of Environment and Energy, South China University of Technology, Guangzhou, Guangdong 510006, China
[d] Department of Chemistry and Biochemistry, University of California, 1156 High Street, Santa Cruz, CA 95064, United States

ARTICLE INFO

Article history:
Received 7 December 2017
Received in revised form
17 January 2018
Accepted 17 January 2018

Keywords:
Selenium
Polyselenide
Lithium battery
Catalysis
Cobalt diselenide

ABSTRACT

The sluggish redox kinetics and dissolution of polyselenide result in severe capacity attenuation of lithium-selenium (Li-Se) batteries, thus significantly limiting its practical application. In this study, we developed a facile annealing procedure to prepare $CoSe_2$-porous carbon composites ($CoSe_2$-PC) as a high-performance cathode material. The formation of $CoSe_2$ nanoparticles in the carbon matrix was confirmed by high resolution transmission electron spectroscopy (HRTEM), X-ray diffraction (XRD) and X-ray photoelectron spectroscopy (XPS) measurements. Se@$CoSe_2$-PC achieved a reversible capacity up to 408 $mAh \cdot g^{-1}$ after 100 charge-discharge cycles at the current rate of 1 C, a performance much higher than that of porous carbon alone. The catalytic effect of $CoSe_2$ on the redox reaction dynamics of polyselenide was examined by cyclic voltammetric measurements using a symmetrical cell of Se@$CoSe_2$-PC in the presence and absence of the polyselenide in the electrolyte, and this likely accounts for the high specific capacity and superior cycle performance of Se@$CoSe_2$-PC based Li-Se batteries. Results from this work may open up a door for suppressing the dissolution of polyselenide and eventually realize Li-Se batteries of high capacity and cycle stability.

1. Introduction

Since Amine's group [1] pioneered the application of Se as a positive electrode for a new class of rechargeable Li batteries in 2012, Li-Se batteries have become a hot topic of research because of several advantages [2–10]. Firstly, selenium (Se) is the congener of elemental S and has similar electrochemical performance to sulfur [1,11,12]. Secondly, the electric conductivity of selenium is 1×10^{-5} $S \cdot m^{-1}$, approximately 20 orders magnitude higher that of sulfur, significantly increasing the utilization of selenium as active cathode materials and thus the energy storage capacity [1,13–15]. The solubility of polyselenide produced during the cycling process is much lower than that of polysulfide in carbonate electrolyte, thus leading to a much weaker shuttle phenomenon of polyselenide and loss of capacity as compared to sulfur [16,17]. Although the theoretical gravimetric capacity of Se is only 675 $mAh \cdot g^{-1}$ [18–20], much lower than that of S (1672 $mAh \cdot g^{-1}$) [21–23], the theoretical volumetric capacity of Se is 3253 $mAh \cdot cm^{-3}$, comparable to that of sulfur (3467 $mAh \cdot cm^{-3}$ based on 2.07 $g \cdot cm^{-3}$) [13,24–26].

Selenium has indeed shown great prospect as an alternative cathode material for lithium batteries, but the dissolution of polyselenide and the large volume change of Se during the charge/discharge process result in a low battery capacity and poor cycle stability [18,27–29], limiting the cycle performance of Li-Se batteries. A number of methods have been explored to overcome this bottleneck for commercialization of Li-Se batteries. Among these, the mostly studied approach is to physically confine Se in microporous carbon spheres [30], ordered mesoporous carbon [10,13], microporous/mesoporous carbon [16,31], hierarchical porous

* Corresponding author.Guangzhou Key Laboratory for Surface Chemistry of Energy Materials, New Energy Research Institute, School of Environment and Energy, South China University of Technology, Guangzhou 510006, China.
** Corresponding author. Department of Chemistry and Biochemistry, University of California, 1156 High Street, Santa Cruz, CA 95064, United States.
E-mail addresses: esxkang@scut.edu.cn (X. Kang), shaowei@ucsc.edu (S. Chen).

https://doi.org/10.1016/j.electacta.2018.01.105
0013-4686/

carbon [32,33], graphene [34–36], etc. The porous structure of the carbon materials not only offer space for the large volume variation of Se during the lithiation/delithiation process, but also suppress the dissolution of polyselenide intermediates in the electrolyte [31,37]. Lately, it has been reported that noble metals, transition metals and transition metal disulfides [38–43] may be used as efficient catalysts to facilitate the polysulfide redox reactions and transform more soluble lithium polysulfide Li_2S_n ($8 \geq n \geq 4$) to less soluble Li_2S_2 and Li_2S in electrolyte, thus enhancing the capacity and cycle performance of the Li-S batteries. However, no such strategy has ever yet been reported to improve the capacity and cycle performance of Li-Se batteries.

Conceptually different from the traditional approach of physical confinement to suppress the dissolution of polyselenide, which usually involve complicated and time-consuming procedures and high energy input to prepare the mesoporous carbon host [10,13,16,31], herein we prepared a porous carbon and cobalt nanoparticles composite (Co-PC) in one-pot reaction and the $CoSe_2$ obtained during the Se melt-diffusion process behaved as redox catalyst and efficiently promoted the transformation of more soluble Li_2Se_n ($8 \geq n \geq 4$) to less soluble Li_2Se in electrolyte, thus suppressing the dissolution of polyselenide and enhancing the capacity and cycle performance. Attributed to this effect, Se@$CoSe_2$-PC achieved 408 $mAh \cdot g^{-1}$ after 100 charge-discharge cycling, superior to that of Se@PC without $CoSe_2$ nanoparticles (233 $mAh \cdot g^{-1}$). This paper demonstrated an alternative strategy of physical confinement to suppress the loss of polyselenide.

2. Experimental section

2.1. Preparation of Co-porous carbon (Co-PC) and porous carbon (PC)

All the chemical reagents were of analytical grade and used without further purification. In a typical procedure, 4 g of ethylenediaminetetraacetic acid (EDTA, Energy Chemicals), 2 g of KOH (Damao Chemical Reagents Factory), and 0.5 g of $Co(NO_3)_2 \cdot 6H_2O$ (Damao Chemical Reagents Factory) were added into an agate mortar and ground for 2 h to obtain a fine mixture. The sample was loaded in a ceramic boat and then directly heated in a horizontal tube furnace under an argon atmosphere. Initially, the mixture was heated up to 100 °C at a heating rate of 2 °C·min^{-1} and kept at this temperature for 1 h, and then further heated up to 700 °C at a heating rate of 3 °C·min^{-1} and maintained at this temperature for 3 h. After cooling down to room temperature in ambient, the obtained black powder was washed with deionized water and absolute ethanol for several times until pH ≈ 7. Finally, the sample was transferred to a drying oven and dried at 70 °C overnight to obtain the Co-PC composite. The PC sample was prepared via the same procedure except that no Co salt was added.

2.2. Loading of Se onto Co-PC and PC

The loading of Se onto the Co-PC composite was carried out via a melt-diffusion method. Firstly, commercial Se powders (Energy Chemicals) and the Co-PC prepared above were thoroughly ground at a mass ratio of 2:1 in a quartz mortar for 1 h to yield a black mixture. Subsequently, the mixture was sealed in a glass tube under an argon atmosphere and heated to 260 °C (heating rate 3 °C·min^{-1} below 215 °C and 0.5 °C·min^{-1} above 215 °C) [25]. A slow heating rate of 0.5 °C·min^{-1} above 215 °C (the melting point of selenium) and a long term dwelling of 12 h at 260 °C were employed to ensure a complete penetration of Se into the porous carbon matrix and the full reaction of elemental Se with Co nanoparticles in Co-PC, leading to the formation of $CoSe_2$ nanoparticles. The Se loaded $CoSe_2$-PC composite was denoted as Se@$CoSe_2$-PC. Se loaded PC composite was synthesized via the same procedure as above and denoted as Se@PC.

2.3. Materials characterization

Thermogravimetric analysis (TGA) was conducted on Mettler Toledo TGA/SDTA851 in N_2 and O_2 atmosphere at the heating rate of 10 °C·min^{-1}. Nitrogen adsorption-desorption isotherms were acquired at 77 K with the Quantachrom Autosorb-1 instrument. X-ray diffraction (XRD) measurements were performed with a Bruker D8 diffractometer with Cu-Kα radiation ($\lambda = 1.5406$ Å). X-ray photoelectron spectra (XPS) was acquired with a Phi X-tool instrument. The morphology of the samples was examined by field-emission scanning electron microscopy (FESEM, Hitachi S-4800) and high-resolution transmission electron microscopy (HRTEM, JEOL TEM-2010).

2.4. Electrochemical measurements

The Se cathode was prepared by a slurry coating procedure. First, the Se@$CoSe_2$-PC composite, carbon black (Super P, Timcal) and water-soluble binder sodium alginate ($(C_6H_7O_6Na)_x$, SA) were mixed at a mass ratio of 80:10:10 to obtain a slurry. Then, the slurry was uniformly pasted onto an aluminum foil using a film applicator, and dried at 70 °C in an electric oven overnight to remove the solvent [44]. The mass loading of active materials for each electrode was estimated to be 1.0–1.2 mg·cm^{-2}.

CR2016-type coin cells were assembled in an argon-filled glove box (Vigor-LG2400/750TS, LTD, Suzhou), in which the oxygen and water contents were less than 1 ppm. The coin cell structure use Se@$CoSe_2$-PC composites as the working electrode, the Li metal with size of 15.6 × 0.45 mm as the counter and reference electrode and the celgard-2400 film as a separator. The electrolyte was 1.0 M $LiPF_6$ in a mixed solvent of ethylene carbonate (EC), ethyl methyl carbonate (EMC) and dimethyl carbonate (DMC) at a volume ratio of 1:1:1. Cyclic voltammetry (CV) and electrochemical impedance spectroscopy (EIS) measurements were carried out with a CHI 660 electrochemical workstation (Shanghai CH Instrument Co., Ltd.) at room temperature.

3. Results and discussion

3.1. Structural analysis

The morphology and surface structure of the resulting Co-PC sample were characterized by SEM and TEM measurements. As shown in Fig. 1 (a), the Co-PC matrix clearly exhibited a three-dimensional structure with microscale inner pores, mainly caused by the etching actions of Co nanoparticles at a high temperature [45]. Further zoom-in in Fig. 1 (b) shows abundant nanometer sized pores on the matte surface of porous carbon, indicating the immense potential for Se confinement and fast ions and electrons transfer [46,47]. The Se@$CoSe_2$-PC composite, obtained by annealing Co-PC in the presence of Se powders at a target temperature under an argon atmosphere, inherited the overall morphology and structure of the pristine Co-PC sample, further suggesting that Se has been uniformly encapsulated into the porous structure of carbon host (Fig. 1 (c)) [31]. The transformation of Co into $CoSe_2$ during the melt-diffusion process was evidenced from the HRTEM image in Fig. 1 (d), where the lattices distance of 0.261 nm was in agreement with that of the (210) plane of pyrite $CoSe_2$ particles.

The transformation of Co to $CoSe_2$ during the melt-diffusion process of Se into Co-PC was further approved by XRD measurements. Fig. 2 (a) displayed three diffraction peaks at $2\theta = 44.21°$,

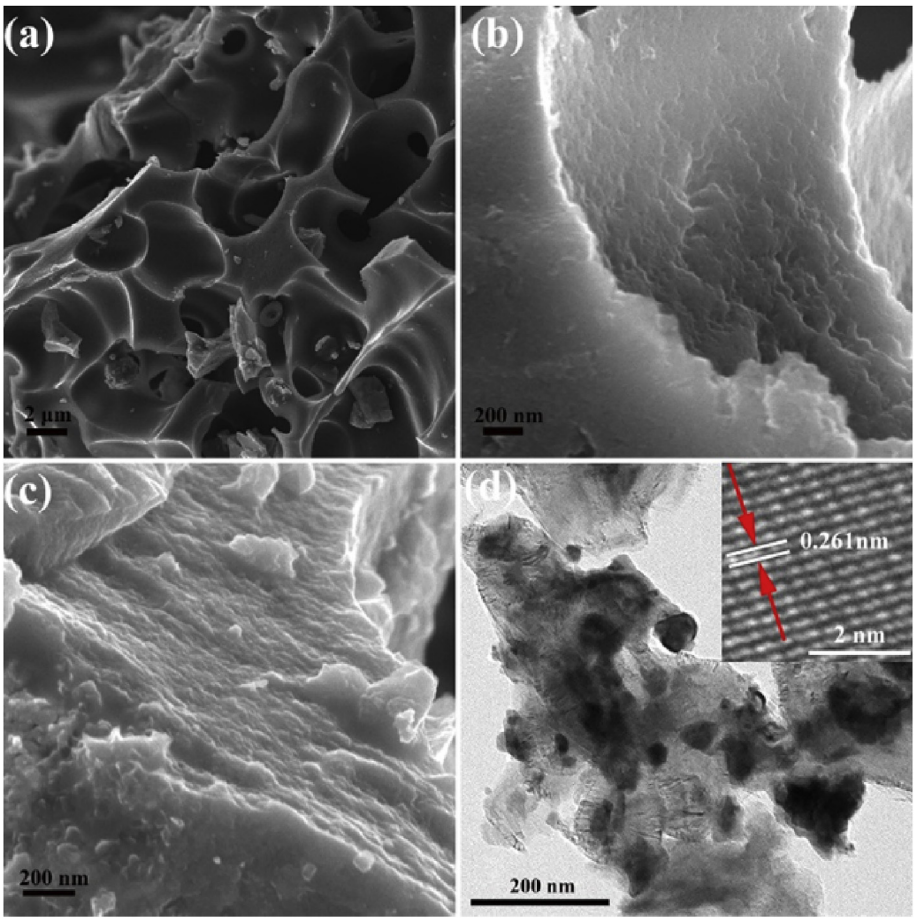

Fig. 1. (a, b) SEM images of Co-PC. (c) SEM image of Se@$CoSe_2$-PC. (d) HRTEM image of Se@$CoSe_2$-PC.

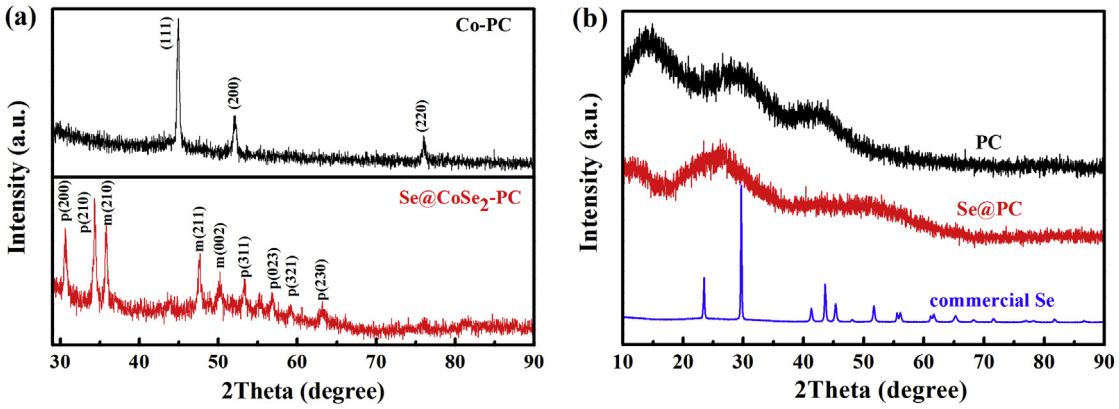

Fig. 2. XRD patterns of (a) Co-PC and Se@$CoSe_2$-PC; and (b) PC and Se@PC.

51.52° and 75.85° for the Co-PC composite, which were attributed to the (111), (200) and (220) lattice facets of metallic Co [39]. Upon the integration of Se into Co-PC at 260 °C, these diffraction peaks vanished while two new sets of diffraction peaks arose, which could be assigned to those of cubic pyrite-structure (ICDD PDF no. 04-003-1990) and macarsite-structure $CoSe_2$ (ICDD PDF no. 00-053-0449) [48,49], suggesting the complete transformation of Co nanoparticles to $CoSe_2$ nanoparticles. From the Bragg's law, the interspacing of the (210) crystalline plane of pyrite $CoSe_2$ was estimated to be 2.601 Å, in good agreement with the value obtained from HRTEM measurement. Interestingly, whereas elemental selenium was successfully loaded into the carbon matrix (as confirmed by TGA measurements, below), no corresponding diffraction peaks for Se were observed in Se@$CoSe_2$-PC (Fig. 2 (a)) or Se@PC (Fig. 2 (b)), indicating that Se was well dispersed into the porous structure of carbon matrix in an amorphous phase [13,20]. Besides, Fig. S1 depicted the Raman spectra of Co-PC and PC. The characteristic D band (1340 cm^{-1}) and G band (1585 cm^{-1}) belonged to disordered carbon and graphitic carbon [14,46,50], respectively. Several bands for Co-PC sample located in the range of

100–700 cm^{-1} could be attributed to the Co nanoparticles [51]. The I_D/I_G values of Co-PC and PC were 0.99 and 0.98, respectively, implying their similar graphitization degree. Upon melt-diffusion treatment of the carbon matrix with Se, the specific surface area decreased dramatically from 1257.5 $m^2 \cdot g^{-1}$ to 6.9 $m^2 \cdot g^{-1}$ for Co-PC and 1567.5 $m^2 \cdot g^{-1}$ to 26.3 $m^2 \cdot g^{-1}$ for PC (Fig. S2), indicating that Se was successfully infused into the porous structure of both Co-PC and PC [19].

The loading of selenium was estimated to be 43 wt% and 51 wt% for Se@$CoSe_2$-PC and Se@PC respectively by TGA in a nitrogen flow, as shown in Fig. 3. (a). The main weight loss between 300 and 600 °C was attributed to the evaporation of elemental Se from the porous carbon matrix. The $CoSe_2$ content in Se@$CoSe_2$-PC was derived from TGA measurements in an O_2 atmosphere, as shown in Fig. 3 (b). According to chemical reaction $3CoSe_2$ (s) + $2O_2$ (g) = Co_3O_4 (s) + 6Se (g), the content of the $CoSe_2$ in the composite was calculated to be 27 wt%. The product of the Se@$CoSe_2$-PC sample after TGA test in O_2 was confirmed to be Co_3O_4 by XRD measurements, as shown in Fig. S3. The gravimetric capacity of Se@$CoSe_2$-PC composite was based on the mass of both elemental selenium and those in $CoSe_2$.

The valence states of Co and Se and the interaction between Se and the carbon matrix in Se@$CoSe_2$-PC and Se@PC were examined by XPS measurements. Fig. 4 (a) displays the full survey spectra of Se@$CoSe_2$-PC and Se@PC, where Co, N and Se were clearly observed for Se@$CoSe_2$-PC. In Fig. 4 (b), the C 1s spectrum displays a main peak at around 284.6 eV, corresponding to graphitic sp^2 carbon [20,39,46]. Meanwhile, the appearance of a peak at 285.4 eV could be ascribed to carbon in C–O bond formed during the annealing process [20]. The high-resolution spectrum of Se 3d electrons in Se@$CoSe_2$-PC was deconvoluted into four sub peaks and displayed in Fig. 4 (c). The two peaks at around 56.2 and 55.4 eV are assigned to the $3d_{3/2}$ and $3d_{5/2}$ electrons of elemental Se [17,20,52], whereas the pair at 55.3 and 54.6 eV were likely due to the Se $3d_{3/2}$ and $3d_{5/2}$ electrons in $CoSe_2$, as observed previously [48]. The broad peak at around 59.0 eV was ascribed to the Se 3d electrons having strong interaction with the porous carbon host through Se–O or Se–C bonds [20]. As illustrated in Fig. S4, the binding energy of Co $2p_{3/2}$ electrons in Se@$CoSe_2$-PC was identified at 778.45 eV, in agreement with that of $CoSe_2$ [48,53].

3.2. Electrochemical characterization

The electrochemical performance of the Se@PC and Se@$CoSe_2$-PC composites as cathode materials for rechargeable Li-Se batteries was evaluated by using 2016-type coin cells assembled with a metallic lithium foil as the counter electrode. To figure out the oxidation/reduction reactions in Li-Se batteries, the three initial cyclic voltammograms were measured for Se@$CoSe_2$-PC and Se@PC between 1.0 and 3.0 V vs Li^+/Li at a scan rate of 0.1 $mV \cdot s^{-1}$, as shown in Fig. 5 (a). Se@PC displayed a pair of cathodic and anodic peaks at 1.58 and 2.12 V in the first voltammetric cycle, corresponding to the reversible one-step reaction of Se to Li_2Se [9,28], which was described by equation: $2Li^+ + Se + 2e^- \leftrightarrow Li_2Se$. In the second cycle, the cathodic peak at 1.58 V was shifted towards a positive potential (1.75 V) due to the electrochemical activation of selenium in the first cycle, associated with a volume expansion and deformation of Se induced by lithiation [16,28]. The appearance of a small peak at 1.68 V was ascribed to the formation of Li_2Se_2 or Li_2Se_n [54], which became a shoulder in the second cycle. In sharp contrast, two cathodic peaks at 1.38 V and 1.57 V and two anodic peaks at 2.15 and 2.33 V in the CV curves were observed for Se@$CoSe_2$-PC. The cathodic peak at 1.38 V and the anodic shoulder at 2.33 V were ascribed to the lithiation and delithiation of $CoSe_2$. Compared to that of Se@PC, no shoulder or sub peak near 1.68 V was observed for Se@$CoSe_2$-PC, indicating that the formation of soluble polyselenide was significantly suppressed due to the presence of $CoSe_2$. The stable and overlapping CV curves in the second and third cycles demonstrated much better cycling performance of Se@$CoSe_2$-PC than Se@PC, possibly due to the suppressed dissolution of polyselenide into the electrolyte and improved utilization of active materials in the cycling process [44,55]. The galvanostatic discharge and charge curves of the Se@$CoSe_2$-PC and Se@PC composites in the potential range of 1.0 and 3.0 V at the current rate at 0.5 C (1 C = 675 $mA \cdot g^{-1}$) were displayed in Fig. 5 (b). Two discharging plateaus at the potentials of 1.4 and 1.75 V for Se@$CoSe_2$-PC can be seen due to the lithiation of $CoSe_2$ and Se, in agreement with the two redox current peaks of CV measurements in Fig. 5 (a). In contrast, only one discharging plateau was observed for Se@PC at 1.75 V, corresponding to the discharging process of Se. Se@$CoSe_2$-PC showed the discharge capacity of 1095 $mAh \cdot g^{-1}$ and a charge capacity of 740 $mAh \cdot g^{-1}$ in the first cycle, at the coulombic efficiency of 67.6%. In the subsequent cycles, nearly 100% coulombic efficiency was achieved owing to the reversible lithiation/delithiation reaction. However, the initial coulombic efficiency of Se@PC is much lower than that of Se@$CoSe_2$-PC, suggesting that $CoSe_2$ played a vital role in maintaining the cycle stability of the Li-Se batteries.

As shown in Fig. 6 (a), the Se@$CoSe_2$-PC sample exhibited excellent rate capability. At the rate of 0.1 C, the initial discharge capacity reached up to 1213 $mAh \cdot g^{-1}$ but declined rapidly due to the activation process at the initial charging and discharging process [56]. The specific capacity gradually degenerated as the current rate increased from 0.1 C to 10 C. The reversible capacity of 631, 509,

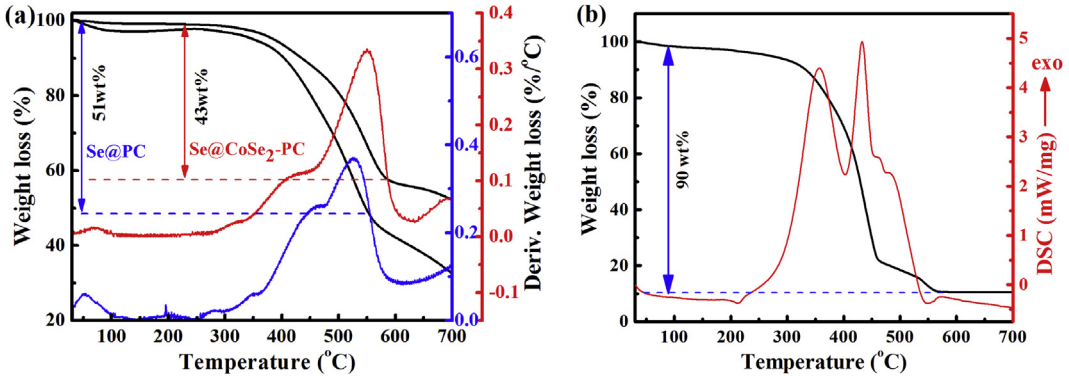

Fig. 3. TGA curves of (a) the Se@PC and Se@$CoSe_2$-PC composites acquired in a N_2 atmosphere and (b) Se@$CoSe_2$-PC composite in an O_2 atmosphere at the heating rate of 10 °C·min^{-1}.

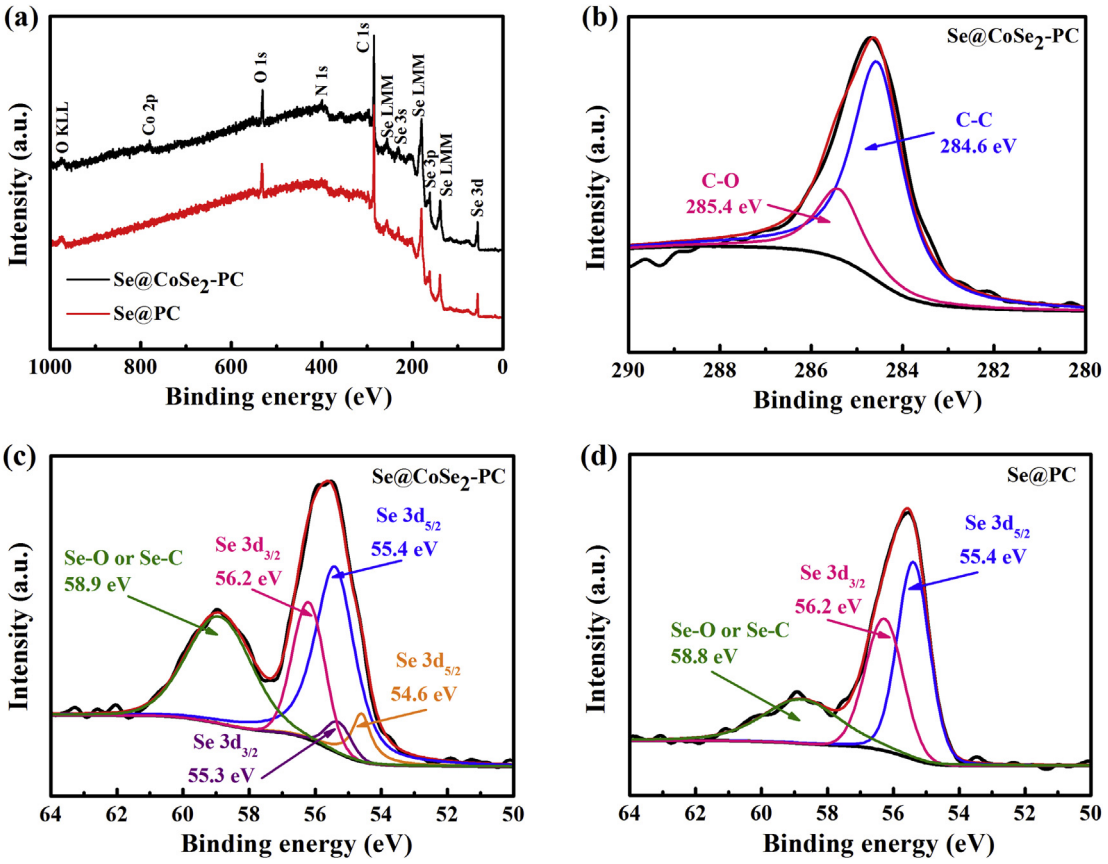

Fig. 4. (a) High-resolution XPS spectra of Se@$CoSe_2$-PC and Se@PC composites. (b) C 1s XPS spectrum of Se@$CoSe_2$-PC. (c, d) Se 3d XPS spectra of Se@$CoSe_2$-PC and Se@PC.

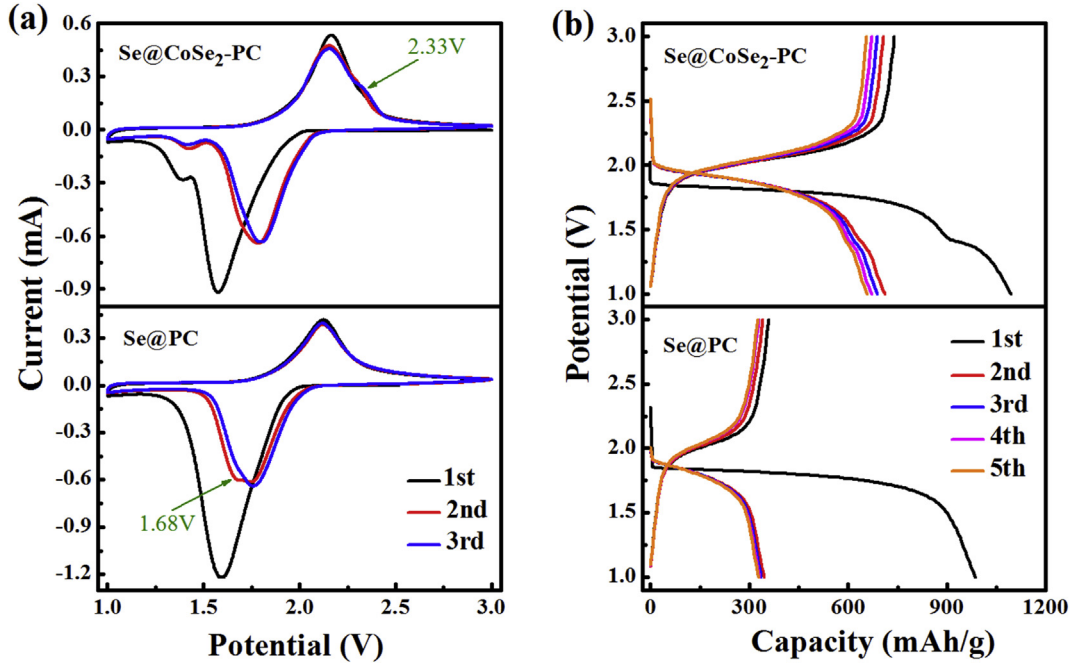

Fig. 5. (a) CV curves of the Se@$CoSe_2$-PC and Se@PC at a scan rate of 0.1 mV·s^{-1} in the voltage range of 3.0–1.0 V vs Li^+/Li. (b) Galvanostatic discharge and charge curves of the Se@$CoSe_2$-PC and Se@PC composites at 0.5C.

428, 356, 275 and 210 mAh·g^{-1} at the current density of 0.2, 0.5, 1, 2, 5 and 10 C, respectively, was retained, comparable to literature values [13,16,31]. When the current rate returned back to 0.1 C, the material recovered most of its specific capacity and retained a value

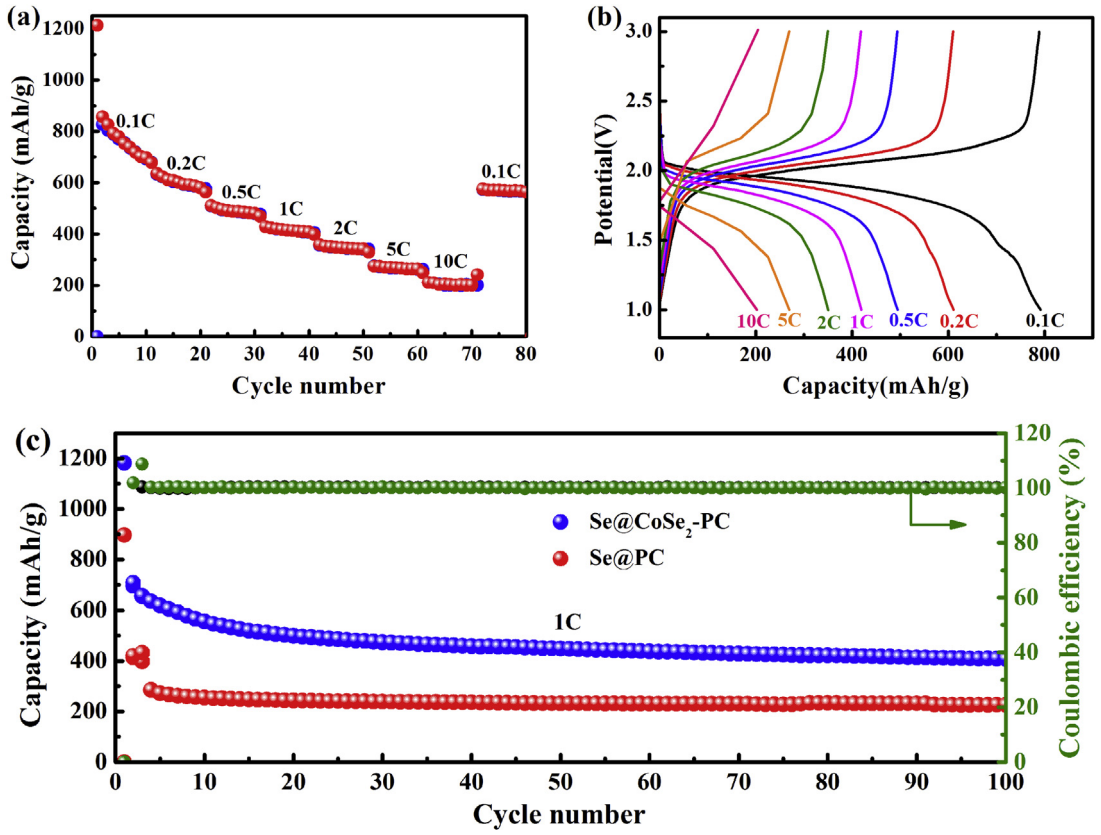

Fig. 6. (a) Rate performance of the Se@$CoSe_2$-PC at increasing current density from 0.1 C to 10 C. (b) The corresponding charge/discharge profiles at various rates. (c) Cycling performance and coulombic efficiency comparisons between the Se@$CoSe_2$-PC and the Se@PC composite electrodes at 1 C.

of 574 mAh·g^{-1}. In contrast, the Se@PC composite exhibited a much lower capacity than Se@$CoSe_2$-PC. In particular, at the large current density of 5 C, it only delivered one third of the specific discharge capacity of Se@$CoSe_2$-PC (96 mAh·g^{-1}) (Fig. S5). Both the discharge and charge capacities of the as-prepared Se@$CoSe_2$-PC composite were preferable at various current densities, demonstrating that $CoSe_2$ plays an important role in improving the specific capacity of the batteries during the electrochemical reaction process. Fig. 6 (b) displays the corresponding charge/discharge voltage profiles at the current rates of 0.1, 0.2, 0.5, 1, 2, 5 and 10 C of the Se@$CoSe_2$-PC electrode in the potential range from 1.0 to 3.0 V. Obviously, the charge/discharge profiles showed enlarged potential difference when the current density increased from 0.1 C to 10 C, as a result of the polarization loss and mechanical energy dissipation during the charge/discharge process [31].

The cycling performance and coulombic efficiency of the Se@$CoSe_2$-PC and Se@PC samples at a current density of 1 C were shown in Fig. 6 (c). The first discharge and charge capacities of the Se@$CoSe_2$-PC composite are 1182 and 696 mAh·g^{-1}, respectively, and the reversible capacity remained at 408 mAh·g^{-1} after 100 cycles along with the coulombic efficiency of 100%, suggesting the high utilization of active materials and effective suppression of the so-called shuttle effect. In contrast, Se@PC only achieved a reversible capacity of 233 mAh·g^{-1} after 100 cycles at the current density of 1 C (red curve in Fig. 6 (c)), far lower than that of Se@$CoSe_2$-PC (408 mAh·g^{-1}). The cycling performance of Se@$CoSe_2$-PC at 0.2 C and 0.5 C was displayed in Fig. S6, demonstrating the discharge capacity of 539 and 454 mAh·g^{-1} in the 100th cycle at the current rates of 0.2 C and 0.5 C. Besides, the SEM images after 100 cycles at 1 C were exhibited in Fig. S7, where the overall structure morphology of the Se@$CoSe_2$-PC composite could be well reserved, suggesting the stability and integrity of the electrode structure [56–59]. The rough surface of Se@$CoSe_2$-PC composite after cycling might be caused by the loss of Se, which was located at the surface and responsible for the capacity loss [60]. Fig. S8 compares the rate performance of the Se@$CoSe_2$-PC with other typical cathode materials for Li-Se battery reported in literature, and the rate capability of Se@$CoSe_2$-PC composite is obviously superior to many of the reported electrode materials, such as Se/GPNF [14], Se/MCN-

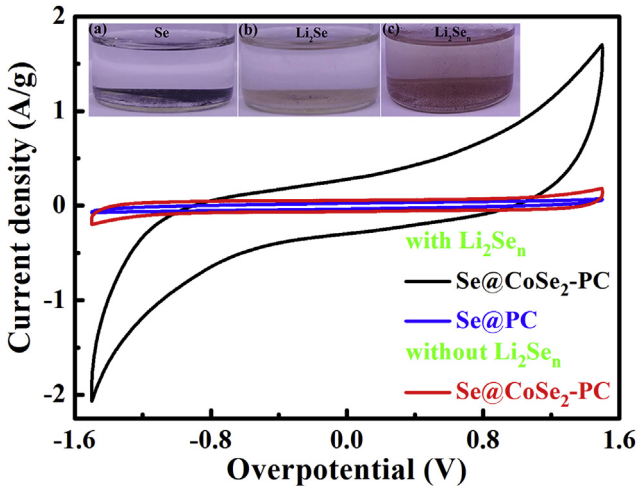

Fig. 7. Polarization curves of the symmetrical cells using Se@$CoSe_2$-PC, Se@PC with and without Li_2Se_n in the electrolyte at a scan rate of 0.1 V·s^{-1}. Insets are the photographs of (a) Se, (b) Li_2Se and (c) combination of the two in the carbonate-based electrolyte.

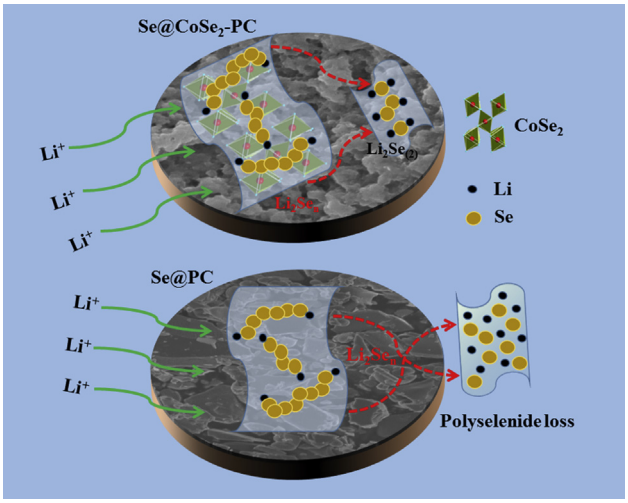

Scheme 1. Illustration of the discharge process in Se-based cathodes. The transformation of polyselenide to Li_2Se was accelerated by $CoSe_2$, suppressing the loss of polyselenide into electrolyte.

RGO [27], NCS/Se-50 [19], Se@C [60], Se_8/C [16], Se@N-CT-48 [37], Se@MICP [31], MHPCS/Se [24] and graphene-CNT@Se [61]. The gravimetric capacity and cycle stability of Se@$CoSe_2$-PC was equally compared with other composites for Li-Se batteries reported in the previous literature and summarized in Table S1. The gravimetric capacity and cycle stability of Se@$CoSe_2$-PC in the current work are competitive to many of the cathode materials reported in the literature. Most importantly, the results of the current work highlighted the role of $CoSe_2$ when introduced into PC, which apparently enhanced both the gravimetric capacity and cycle stability of Se@$CoSe_2$-PC cathode material in relative to that of Se@PC without $CoSe_2$.

Zhang and coworkers [41] have reported that CoS_2 in sulfiphilic host effectively propelled the redox reaction of polysulfide, suppressed the dissolution of polysulfide and remarkably improved the utilization of active materials. It has been widely accepted that the poor capacity and cycle performance of Se@PC in lithium batteries was mainly caused by the dissolution of polyselenide into the ether-based electrolyte [62]. Thus, we speculate that the dissolution of polyselenide into the carbonate-based electrolyte might be responsible for the poor cycle performance of Se@PC and $CoSe_2$ in Se@$CoSe_2$-PC composite might play similar role to that of CoS_2 in sulfiphilic matrix, facilitating the redox reaction of polyselenide and further improving the capacity of the Li-Se batteries.

In order to simulate the possible polyselenide products in the carbonate-based electrolyte, we added 5 mg of Se and 5 mg of Li_2Se respectively into two separate vials containing 5 mL electrolyte. As shown in the inset (a) and (b) to Fig. 7, only clear and colourless solution was observed for the vials containing Se and Li_2Se respectively, indicating that Se or Li_2Se is barely soluble in carbonate-based electrolyte. In sharp contrast, clear and light-brown solution was obtained for the vial containing both Se and Li_2Se in the inset (c) of Fig. 7, indicating the formation of polyselenide solution in the carbonate-based electrolyte. Although the brown colour of polyselenide in carbonate-based electrolyte is much lighter than that in ether-based electrolyte [17], which might indicate much less solubility of polyselenide in carbonate-based electrolyte than in ether-based electrolyte, the dissolution of polyselenide to carbonate-based electrolyte is still appreciable and might be responsible for the loss of active materials and battery capacity.

To further investigate the electrocatalytic activity of $CoSe_2$ towards the redox kinetics of polyselenide, symmetrical cells were assembled by sandwiching the electrolyte with or without Li_2Se_n between two identical electrodes of Se@$CoSe_2$-PC as working and counter electrodes. The open circuit voltages of the designed symmetrical cells were measured to be 0 V. CV tests for the symmetrical cells were performed within the voltage window of −1.5 to 1.5 V at the scan rate of 0.1 $V \cdot s^{-1}$. The polarization profiles are essentially featureless when $CoSe_2$ is missing in the electrode material or the electrolyte is absent from Li_2Se_n (Fig. 7). In contrast, the current density increased remarkably in the Se@$CoSe_2$-PC symmetrical cells using the Li_2Se_n-containing electrolyte, demonstrating that $CoSe_2$ particles likely triggered and dynamically accelerated the redox reactions of lithium polyselenide, as illustrated in Scheme 1. Similar to that in symmetrical cells, in fully assembled Li-Se batteries with Se@$CoSe_2$-PC cathodes, $CoSe_2$ might significantly accelerate the redox kinetics of more soluble polyselenide to less soluble Li_2Se on PC, thus alleviating the dissolution of polyselenide into the electrolyte and thus reducing the loss of active materials.

The cycle stability of the cells was strongly related with the interfacial charge transfer and lithium ion diffusion in the cathode materials. Thus electrochemical impedance spectroscopy (EIS) studies were conducted to understand the electrochemical performance of Se@PC and Se@$CoSe_2$-PC. Fig. 8 (a) and (b) display the Nyquist plots (dotted lines) for Se@$CoSe_2$-PC and Se@PC, which were fitted (solid lines) with the equivalent circuit shown in the inset to Fig. 8 (b). R_s, R_{ct} and W_o represent the electrolyte resistance, interfacial charge transfer resistance and Warburg resistance [18,19,63], which was associated with the lithium ion diffusion in

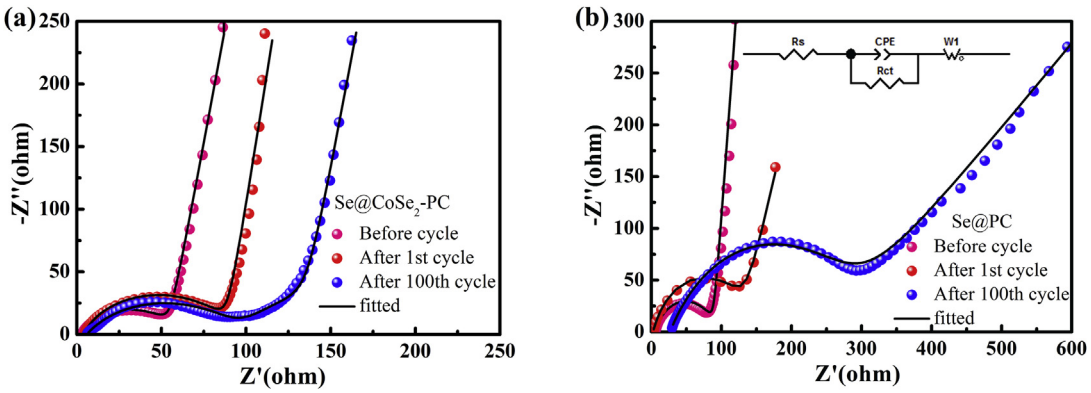

Fig. 8. Nyquist plots of (a) Se@$CoSe_2$-PC and (b) Se@PC based cells in the frequency range of 100 kHz-100 mHz. The inset in panel (b) is the equivalent circuit fitting the EIS spectra.

active materials [64]. The fitting parameters were listed in Table S2. R_{ct} was quantified by the *x*-axis intersect of the semicircle in the high-frequency domain, while W_o was represented by the straight line in the low-frequency region [65]. Upon cycling, the increase of the interfacial charge transfer resistance could be attributed to the decomposition of electrolyte on the electrode surface and the volume variation [16,17]. In fact, R_{ct} for Se@PC was increased to 122.8 Ω after the first cycle and to 238.4 Ω after the 100th cycle. In contrast, R_{ct} of Se@$CoSe_2$-PC changed from 51.5 to 83.5 Ω after the first cycle and then remained almost constant even after 100th cycle, indicating that the interfacial charge transfer of Se@$CoSe_2$-PC was much faster and more stable than that of Se@PC [18,66–68].

4. Conclusion

In summary, a Se@$CoSe_2$-PC composite was prepared by a facile chemistry approach and used as a high-performance cathode material for Li-Se batteries, where $CoSe_2$ served as an effective electrocatalyst and dynamically facilitated the redox reaction kinetics of polyselenide and suppressed the dissolution of Li_2Se_n intermediates into the electrolyte, thus mitigating the shuttle effect. Because of the catalytic effect of $CoSe_2$, Se@$CoSe_2$-PC retained a reversible capacity of 408 mAh·g^{-1} at the current rate of 1 C after 100 charge-discharge cycles, much higher than that of 233 mAh·g^{-1} achieved by Se@PC without the $CoSe_2$ catalyst. Polyselenide was demonstrated to be soluble in the carbonate-based electrolyte. The catalytic activity of $CoSe_2$ towards polyselenide was demonstrated by the polarization of symmetrical cell: Se@$CoSe_2$-PC in the presence of polyselenide displayed a much higher polarization current than that without polyselenide in the electrolyte or Se@PC in the presence of polyselenide in the electrolyte. The concise but efficient amelioration of the Se-containing cathode material might offer an innovative strategy to promote the overall electrochemical performance of high-energy rechargeable Li-Se battery.

Conflicts of interest

There are no conflicts of interest to declare.

Acknowledgement

This work was supported by the National Natural Science Foundation of China (No. 51602106) and the Fundamental Research Funds for Central Universities (SCUT Grant No. 2017MS066).

Appendix A. Supplementary data

Supplementary data related to this article can be found at https://doi.org/10.1016/j.electacta.2018.01.105.

References

[1] A. Abouimrane, D. Dambournet, K.W. Chapman, P.J. Chupas, W. Weng, K. Amine, A new class of lithium and sodium rechargeable batteries based on selenium and selenium-sulfur as a positive electrode, J. Am. Chem. Soc. 134 (2012) 4505–4508.
[2] J.T. Xu, J.M. Ma, Q.H. Fan, S.J. Guo, S.X. Dou, Recent progress in the design of advanced cathode materials and battery models for high-performance lithium-X (X = O-2, S, Se, Te, I-2, Br-2) batteries, Adv. Mater. 29 (2017), 1606454.
[3] J. Ding, H. Zhou, H.L. Zhang, T. Stephenson, Z. Li, D. Karpuzov, D. Mitlin, Exceptional energy and new insight with a sodium-selenium battery based on a carbon nanosheet cathode and a pseudographite anode, Energy Environ. Sci. 10 (2017) 153–165.
[4] J.T. Zhang, Z. Li, X.W. Lou, A freestanding selenium disulfide cathode based on cobalt disulfide-decorated multichannel carbon fibers with enhanced lithium storage performance, Angew. Chem. Int. Ed. 56 (2017) 14107–14112.
[5] J.R. He, W.Q. Lv, Y.F. Chen, J. Xiong, K.C. Wen, C. Xu, W.L. Zhang, Y.R. Li, W. Qin, W.D. He, Three-dimensional hierarchical C-Co-N/Se derived' from metal-organic framework as superior cathode for Li-Se batteries, J. Power Sources 363 (2017) 103–109.
[6] L.C. Zeng, W.C. Zeng, Y. Jiang, X. Wei, W.H. Li, C.L. Yang, Y.W. Zhu, Y. Yu, A flexible porous carbon nanofibers-selenium cathode with superior electrochemical performance for both Li-Se and Na-Se batteries, Adv. Eng. Mater. 5 (2015).
[7] B. Kalimuthu, K. Nallathamby, Designed formulation of Se-Impregnated N-Containing hollow core mesoporous shell carbon spheres: multifunctional potential cathode for Li-Se and Na-Se batteries, ACS Appl. Mater. Interfaces 9 (2017) 26756–26770.
[8] J. Jin, X.C. Tian, N. Srikanth, L.B. Kong, K. Zhou, Advances and challenges of nanostructured electrodes for Li-Se batteries, J. Mater. Chem. 5 (2017) 10110–10126.
[9] Y. Jiang, X.J. Ma, J.K. Feng, S.L. Xiong, Selenium in nitrogen-doped microporous carbon spheres for high-performance lithium-selenium batteries, J. Mater. Chem. 3 (2015) 4539–4546.
[10] C. Zheng, M.Y. Liu, W.Q. Chen, L.X. Zeng, M.D. Wei, An in situ formed Se/CMK-3 composite for rechargeable lithium-ion batteries with long-term cycling performance, J. Mater. Chem. 4 (2016) 13646–13651.
[11] C.P. Yang, Y.X. Yin, Y.G. Guo, Elemental selenium for electrochemical energy storage, J. Phys. Chem. Lett. 6 (2015) 256–266.
[12] I. Gomez, D. Mantione, O. Leonet, J.A. Blazquez, D. Mecerreyes, Hybrid Sulfur–Selenium Co-polymers as cathodic materials for lithium batteries, Chemelectrochem 4 (2017) 1–7.
[13] C.P. Yang, S. Xin, Y.X. Yin, H. Ye, J. Zhang, Y.G. Guo, An advanced selenium-carbon cathode for rechargeable lithium-selenium batteries, Angew. Chem. Int. Ed. 52 (2013) 8363–8367.
[14] R. Mukkabla, S. Deshagani, P. Meduri, M. Deepa, P. Ghosal, Selenium/graphite platelet nanofiber composite for durable Li-Se batteries, ACS Energy Lett. 2 (2017) 1288–1295.
[15] Z. Li, L.X. Yuan, Z.Q. Yil, Y. Liu, Y.H. Huang, Confined selenium within porous carbon nanospheres as cathode for advanced Li-Se batteries, Nano Energy 9 (2014) 229–236.
[16] C. Luo, Y.H. Xu, Y.J. Zhu, Y.H. Liu, S.Y. Zheng, Y. Liu, A. Langrock, C.S. Wang, Selenium@Mesoporous carbon composite with superior lithium and sodium storage capacity, ACS Nano 7 (2013) 8003–8010.
[17] Y.J. Cui, A. Abouimrane, J. Lu, T. Bolin, Y. Ren, W. Weng, C.J. Sun, V.A. Maroni, S.M. Heald, K. Amine, (De)Lithiation mechanism of Li/SeSx (x=0-7) batteries determined by in situ synchrotron x-ray diffraction and x-ray absorption spectroscopy, J. Am. Chem. Soc. 135 (2013) 8047–8056.
[18] Q.F. Cai, Y.Y. Li, L. Wang, Q.W. Li, J. Xu, B. Gao, X.M. Zhang, K.F. Huo, P.K. Chu, Freestanding hollow double-shell Se@CNx nanobelts as large-capacity and high-rate cathodes for Li-Se batteries, Nano Energy 32 (2017) 1–9.
[19] Z.Q. Li, L.W. Yin, MOF-derived, N-doped, hierarchically porous carbon sponges as immobilizers to confine selenium as cathodes for Li-Se batteries with superior storage capacity and perfect cycling stability, Nanoscale 7 (2015) 9597–9606.
[20] X.N. Li, J.W. Liang, Z.G. Hou, W.Q. Zhang, Y. Wang, Y.C. Zhu, Y.T. Qian, A new salt-baked approach for confining selenium in metal complex-derived porous carbon with superior lithium storage properties, Adv. Funct. Mater. 25 (2015) 5229–5238.
[21] P.T. Dirlam, R.S. Glass, K. Char, J. Pyun, The use of polymers in Li-S batteries: a review, J. Polym. Sci. Polym. Chem. 55 (2017) 1635–1668.
[22] I. Gomez, D. Mecerreyes, J.A. Blazquez, O. Leonet, H. Ben Youcef, C. Li, J.L. Gómez-Cámer, O. Bondarchuk, L. Rodriguez-Martinez, Inverse vulcanization of sulfur with divinylbenzene: stable and easy processable cathode material for lithium-sulfur batteries, J. Power Sources 329 (2016) 72–78.
[23] W.J. Chung, J.J. Griebel, E.T. Kim, H. Yoon, A.G. Simmonds, H.J. Ji, P.T. Dirlam, R.S. Glass, J.J. Wie, N.A. Nguyen, B.W. Guralnick, J. Park, A. Somogyi, P. Theato, M.E. Mackay, Y.E. Sung, K. Char, J. Pyun, The use of elemental sulfur as an alternative feedstock for polymeric materials, Nat. Chem. 5 (2013) 518–524.
[24] T. Liu, C.L. Dai, M. Jia, D.Y. Liu, S.J. Bao, J. Jiang, M.W. Xu, C.M. Li, Selenium embedded in metal-organic framework derived hollow hierarchical porous carbon spheres for advanced lithium-selenium batteries, ACS Appl. Mater. Interfaces 8 (2016) 16063–16070.
[25] S. Xin, L. Yu, Y. You, H.P. Cong, Y.X. Yin, X.L. Du, Y.G. Guo, S.H. Yu, Y. Cui, J.B. Goodenough, The electrochemistry with lithium versus sodium of selenium confined to slit micropores in carbon, Nano Lett. 16 (2016) 4560–4568.
[26] H. Zhang, D.D. Jia, Z.W. Yang, F.Q. Yu, Y.L. Su, D.J. Wang, Q. Shen, Alkaline lignin derived porous carbon as an efficient scaffold for lithium-selenium battery cathode, Carbon 122 (2017) 547–555.
[27] K. Han, Z. Liu, J.M. Shen, Y.Y. Lin, F. Dai, H.Q. Ye, A free-standing and ultralong-life lithium-selenium battery cathode enabled by 3D mesoporous carbon/graphene hierarchical architecture, Adv. Funct. Mater. 25 (2015) 455–463.
[28] J.J. Zhang, L. Fan, Y.C. Zhu, Y.H. Xu, J.W. Liang, D.H. Wei, Y.T. Qian, Selenium/interconnected porous hollow carbon bubbles composites as the cathodes of Li-Se batteries with high performance, Nanoscale 6 (2014) 12952–12957.
[29] J.J. Zhou, J. Yang, Z.X. Xu, T. Zhang, Z.Y. Chen, J.L. Wang, A high performance lithium-selenium battery using a microporous carbon confined selenium cathode and a compatible electrolyte, J. Mater. Chem. 5 (2017) 9350–9357.
[30] C. Wu, L.X. Yuan, Z. Li, Z.Q. Yi, R. Zeng, Y.R. Li, Y.H. Huang, High-performance lithium-selenium battery with Se/microporous carbon composite cathode and carbonate-based electrolyte, Sci. China Math. 58 (2015) 91–97.

[31] Y.X. Liu, L. Si, X.S. Zhou, X. Liu, Y. Xu, J.C. Bao, Z.H. Dai, A selenium-confined microporous carbon cathode for ultrastable lithium-selenium batteries, J. Mater. Chem. 2 (2014) 17735–17739.
[32] S.F. Jiang, Z. Zhang, Y.Q. Lai, Y.H. Qu, X.W. Wang, J. Li, Selenium encapsulated into 3D interconnected hierarchical porous carbon aerogels for lithium-selenium batteries with high rate performance and cycling stability, J. Power Sources 267 (2014) 394–404.
[33] Y.H. Qu, Z.A. Zhang, S.F. Jiang, X.W. Wang, Y.Q. Lai, Y.X. Liu, J. Li, Confining selenium in nitrogen-containing hierarchical porous carbon for high-rate rechargeable lithium-selenium batteries, J. Mater. Chem. 2 (2014) 12255–12261.
[34] X. Peng, L. Wang, X.M. Zhang, B. Gao, J.J. Fu, S. Xiao, K.F. Huo, P.K. Chu, Reduced graphene oxide encapsulated selenium nanoparticles for high-power lithium-selenium battery cathode, J. Power Sources 288 (2015) 214–220.
[35] J.R. He, Y.F. Chen, W.Q. Lv, K.C. Wen, P.J. Li, Z.G. Wang, W.L. Zhang, W. Qin, W.D. He, Three-dimensional hierarchical graphene-CNT@Se: a highly efficient freestanding cathode for Li-Se batteries, ACS Energy Lett 1 (2016) 16–20.
[36] J.J. Zhang, Y.H. Xu, L. Fan, Y.C. Zhu, J.W. Liang, Y.T. Qian, Graphene-encapsulated selenium/polyani line core-shell nanowires with enhanced electrochemical performance for Li-Se batteries, Nano Energy 13 (2015) 592–600.
[37] D.B. Babu, K. Ramesha, Constraining polyselenide formation in ether based electrolytes through confinement of Se in microporous carbon matrix for Li-Se batteries, Electrochim. Acta 219 (2016) 295–304.
[38] H. Al Salem, G. Babu, C.V. Rao, L.M.R. Arava, Electrocatalytic polysulfide traps for controlling redox shuttle process of Li-S batteries, J. Am. Chem. Soc. 137 (2015) 11542–11545.
[39] Y.J. Li, J.M. Fan, M.S. Zheng, Q.F. Dong, A novel synergistic composite with multi-functional effects for high-performance Li-S batteries, Energy Environ. Sci. 9 (2016) 1998–2004.
[40] Y. Li, J. Fan, J. Zhang, J. Yang, R. Yuan, J. Chang, M. Zheng, Q. Dong, A honeycomb-like Co@N–C composite for ultrahigh sulfur loading Li–S batteries, ACS Nano 11 (2017) 11417–11424.
[41] Z. Yuan, H.J. Peng, T.Z. Hou, J.Q. Huang, C.M. Chen, D.W. Wang, X.B. Cheng, F. Wei, Q. Zhang, Powering lithium-sulfur battery performance by propelling polysulfide redox at sulfiphilic hosts, Nano Lett. 16 (2016) 519–527.
[42] C. Ye, L. Zhang, C.X. Guo, D.D. Li, A. Vasileff, H.H. Wang, S.Z. Qiao, A 3D hybrid of chemically coupled nickel sulfide and hollow carbon spheres for high performance lithium-sulfur batteries, Adv. Funct. Mater. 27 (2017), 1702524.
[43] Z. Li, J.T. Zhang, B.Y. Guan, D. Wang, L.M. Liu, X.W. Lou, A sulfur host based on titanium monoxide@carbon hollow spheres for advanced lithium-sulfur batteries, Nat. Commun. 7 (2016), 13065.
[44] T. Liu, Y. Zhang, J.K. Hou, S.Y. Lu, J. Jiang, M.W. Xu, High performance mesoporous C@Se composite cathodes derived from Ni-based MOFs for Li-Se batteries, RSC Adv. 5 (2015) 84038–84043.
[45] Y. Chen, J. Dong, L. Qiu, X. Li, Q. Li, H. Wang, S. Liang, H. Yao, H. Huang, H. Gao, J.-K. Kim, F. Ding, L. Zhou, A catalytic etching-wetting-dewetting mechanism in the formation of hollow graphitic carbon fiber, Inside Chem. 2 (2017) 299–310.
[46] Y.M. Chen, X.Y. Li, K. Park, L.M. Zhou, H.T. Huang, Y.W. Mai, J.B. Goodenough, Hollow nanotubes of N-Doped carbon on CoS, Angew. Chem. Int. Ed. 55 (2016) 15831–15834.
[47] J. Park, E.T. Kim, C. Kim, J. Pyun, H.S. Jang, J. Shin, J.W. Choi, K. Char, Y.E. Sung, The importance of confined sulfur nanodomains and adjoining electron conductive pathways in subreaction regimes of Li-S batteries, Adv Energy Mater. 7 (2017), 1700074.
[48] D.S. Kong, H.T. Wang, Z.Y. Lu, Y. Cui, CoSe2 nanoparticles grown on carbon fiber paper: an efficient and stable electrocatalyst for hydrogen evolution reaction, J. Am. Chem. Soc. 136 (2014) 4897–4900.
[49] R.S. Sun, M.K.Y. Chan, G. Ceder, First-principles electronic structure and relative stability of pyrite and marcasite: implications for photovoltaic performance, Phys. Rev. B 83 (2011), 235311.
[50] T. Chen, B.R. Cheng, G.Y. Zhu, R.P. Chen, Y. Hu, L.B. Ma, H.L. Lv, Y.R. Wang, J. Liang, Z.X. Tie, Z. Jin, J. Liu, Highly efficient retention of polysulfides in "sea urchin"-like carbon nanotube/nanopolyhedra superstructures as cathode material for ultralong-life lithium-sulfur batteries, Nano Lett. 17 (2017) 437–444.
[51] W.J. Zhou, J. Lu, K. Zhou, L.J. Yang, Y.T. Ke, Z.H. Tang, S.W. Chen, CoSe2 nanoparticles embedded defective carbon nanotubes derived from MOFs as efficient electrocatalyst for hydrogen evolution reaction, Nano Energy 28 (2016) 143–150.
[52] H. Ye, Y.X. Yin, S.F. Zhang, Y.G. Guo, Advanced Se-C nanocomposites: a bifunctional electrode material for both Li-Se and Li-ion batteries, J. Mater. Chem. 2 (2014) 13293–13298.
[53] J. Yang, G.H. Cheng, J.H. Zeng, S.H. Yu, X.M. Liu, Y.T. Qian, Shape control and characterization of transition metal diselenides MSe2 (M = Ni, Co, Fe) prepared by a solvothermal-reduction process, Chem. Mater. 13 (2001) 848–853.
[54] C.H. Zhao, S.Z. Fang, Z.B. Hu, S.E. Qiu, K.Y. Liu, Synthesis of selenium/EDTA-derived porous carbon composite as a Li-Se battery cathode, J. Nanoparticle Res. 18 (2016) 201.
[55] J. Li, X.X. Zhao, Z. Zhang, Y.Q. Lai, Facile synthesis of hollow carbonized polyaniline spheres to encapsulate selenium for advanced rechargeable lithium-selenium batteries, J. Alloy. Comp. 619 (2015) 794–799.
[56] J. Ding, H. Zhou, H. Zhang, L. Tong, D. Mitlin, Selenium impregnated monolithic carbons as free-standing cathodes for high volumetric energy lithium and sodium metal batteries, Adv. Eng. Mater. (2017), 1701918.
[57] X.Y. Li, Y.M. Chen, H.T. Wang, H.M. Yao, H.T. Huang, Y.W. Mai, N. Hu, L.M. Zhou, Inserting Sn nanoparticles into the pores of TiO2-x-C nanofibers by lithiation, Adv. Funct. Mater. 26 (2016) 376–383.
[58] V.P. Oleshko, A.A. Herzing, K.A. Twedt, J.J. Griebe, J.J. McClelland, J. Pyun, C.L. Soles, Multimodal characterization of the morphology and functional interfaces in composite electrodes for Li-S batteries by Li ion and electron beams, Langmuir 33 (2017) 9361–9377.
[59] Y. Chen, X. Li, K. Park, W. Lu, C. Wang, W. Xue, F. Yang, J. Zhou, L. Suo, T. Lin, H. Huang, J. Li, J.B. Goodenough, Nitrogen-Doped carbon for sodium-ion battery anode by self-etching and graphitization of bimetallic MOF-based composite, Inside Chem. 3 (2017) 152–163.
[60] J. Guo, Q.S. Wang, C. Qi, J. Jin, Y.J. Zhu, Z.Y. Wen, One-step microwave synthesized core-shell structured selenium@carbon spheres as cathode materials for rechargeable lithium batteries, Chem. Commun. 52 (2016) 5613–5616.
[61] K. Han, Z. Liu, H.Q. Ye, F. Dai, Flexible self-standing graphene-Se@CNT composite film as a binder-free cathode for rechargeable Li-Se batteries, J. Power Sources 263 (2014) 85–89.
[62] L.C. Zeng, W.H. Li, Y. Jiang, Y. Yu, Recent progress in Li-S and Li-Se batteries, Rare Met. 36 (2017) 339–364.
[63] C. Luo, Y.J. Zhu, Y. Wen, J.J. Wang, C.S. Wang, Carbonized polyacrylonitrile-stabilized SeSx cathodes for long cycle life and high power density lithium ion batteries, Adv. Funct. Mater. 24 (2014) 4082–4089.
[64] Y.X. Liu, L. Si, Y.C. Du, X.S. Zhou, Z.H. Dai, J.C. Bao, Strongly bonded selenium/microporous carbon nanofibers composite as a high-performance cathode for lithium-selenium batteries, J. Phys. Chem. C 119 (2015) 27316–27321.
[65] T. Wang, S.J. Shi, Y.H. Li, M.X. Zhao, X.F. Chang, D. Wu, H.Y. Wang, L.M. Peng, P. Wang, G. Yang, Study of microstructure change of carbon nanofibers as binder-free anode for high-performance lithium-ion batteries, ACS Appl. Mater. Interfaces 8 (2016) 33091–33101.
[66] J.M. Zheng, J. Tian, D.X. Wu, M. Gu, W. Xu, C.M. Wang, F. Gao, M.H. Engelhard, J.G. Zhang, J. Liu, J. Xiao, Lewis acid-base interactions between polysulfides and metal organic framework in lithium sulfur batteries, Nano Lett. 14 (2014) 2345–2352.
[67] R. Demir-Cakan, M. Morcrette, Gangulibabu, A. Gueguen, R. Dedryvere, J.M. Tarascon, Li-S batteries: simple approaches for superior performance, Energy Environ. Sci. 6 (2013) 176–182.
[68] J.M. Zheng, M. Gu, C.M. Wang, P.J. Zuo, P.K. Koech, J.G. Zhang, J. Liu, J. Xiao, Controlled nucleation and growth process of Li2S2/Li2S in lithium-sulfur batteries, J. Electrochem. Soc. 160 (2013) A1992–A1996.